Journal of Solid State Chemistry 183 (2010) 1726–1732

Contents lists available at ScienceDirect

Journal of Solid State Chemistry

journal homepage: www.elsevier.com/locate/jssc

Structural, magnetic, and electrochemical studies on lithium insertion materials $LiNi_{1-x}Co_xO_2$ with $0 \le x \le 0.25$

Kazuhiko Mukai *, Jun Sugiyama, Yoshifumi Aoki

Toyota Central Research and Development Laboratories, Inc., 41-1 Yokomichi, Nagakute, Aichi 480-1192, Japan

ARTICLE INFO

Article history:
Received 22 February 2010
Received in revised form
7 May 2010
Accepted 17 May 2010
Available online 26 May 2010

Keywords:
Lithium-ion battery
Lithium nickel cobalt oxide
Magnetism

ABSTRACT

The structural, magnetic, and electrochemical properties of the $LiNi_{1-x}Co_xO_2$ samples with $x=0$, 0.05, 0.1, and 0.25 have been investigated by powder X-ray diffraction analyses, magnetic susceptibility (χ) measurements, and electrochemical charge and discharge test in non-aqueous lithium cell. According to the structural analyses using a Rietveld method, the occupancy of the Ni ions in the Li layer was estimated to be below 0.01 for all the samples and was eventually independent of x. The temperature (T) dependence of χ^{-1} obtained with the magnetic field $H=10$ kOe indicated that all the samples are a Curie–Weiss paramagnet down to ~ 100 K. At low T, all the samples entered into a spin-glass-like phase below T_f. The magnitude of T_f was found to decrease almost linearly with x, as in the case for the x dependences of the lattice parameters of a_h- and c_h-axes, Weiss temperature, and effective magnetic moment. It is, therefore, found that the change of the magnetic properties with x is simply explained by a dilution effect due to the increase of the quantity of Co^{3+} ions. On the other hand, the electrochemical measurements demonstrated that the irreversible capacity at the initial cycle is drastically decreased by the small amount of Co ions. Furthermore, the discharge capacity (Q_{dis}) for the $x=0.05$ and 0.1 samples are larger than that for the $x=0$ sample; namely, $Q_{dis}=180$ mAh g^{-1} for $x=0$, $Q_{dis}=217$ mAh g^{-1} for $x=0.05$, and $Q_{dis}=206$ mAh g^{-1} for $x=0.1$. Comparing with the past results, the amount of Ni ions in the Li layer is found to play a significant role for determining the magnetic and electrochemical properties of $LiNi_{1-x}Co_xO_2$.

1. Introduction

In order to reduce carbon dioxide in an exhaust gas of automobiles and improve their fuel consumption rate, lithium-ion batteries (LIB) with high energy-density and long cycle-life have been eagerly investigated since 1990's [1]. In particular, a development of new positive electrode materials is thought to be crucial for LIB to increase the energy-density and to elongate the cycle-life. Among many positive electrode materials, a stoichiometric $LiNiO_2$ [2,3] and lightly Co-substituted $LiNiO_2$, i.e. $LiNi_{1-x}Co_xO_2$ with $x \le 0.25$ [4,5], are attractive for the LIB with high energy-density, because their rechargeable capacity ranges about 170 mAh g^{-1} below 4.2 V. Since both $LiNiO_2$ and $LiCoO_2$ adopt a layered structure with a space group of $R\bar{3}m$, $LiNi_{1-x}Co_xO_2$ is known to be a solid solution between $LiNiO_2$ and $LiCoO_2$ in the whole x range [4–8]. This was evidenced by the fact that the lattice parameters for $LiNi_{1-x}Co_xO_2$ follow a Vegard's law, namely, as x increases from 0 to 1, the hexagonal lattice parameters of a_h- and c_h-axes decrease monotonically [4,6–8]. This means that Ni^{3+} ions and Co^{3+} ions distribute randomly in the transition metal layer.

However, magnetic susceptibility (χ) measurements, which are very sensitive to the (local)structure, exhibited a complex magnetic nature especially for $x<0.25$ [7–9]. That is, the temperature (T) dependence of χ^{-1} for the $x=0.05$, 0.10 and 0.15 compounds indicated the appearance of either a ferromagnetic (FM) or ferrimagnetic component below ~ 200 K [7], although the $\chi^{-1}(T)$ curve for $LiNiO_2$ showed a Curie–Weiss paramagnetic (PM) behavior down to ~ 100 K [10]. Furthermore, the effective magnetic moments (μ_{eff}) for these compounds were found to be ~ 1.5 times larger than the predicted value (μ_{eff}^{pre}), under the assumption that Ni^{3+} ions and Co^{3+} ions are in the low-spin state with $S=\frac{1}{2}$ ($t_{2g}^6 e_g^1$) and $S=0$ (t_{2g}^6), respectively [7]. This implies that a large amount of Ni ions exists in the Li layer, because χ^{-1} for $Li_{0.76}Ni_{1.24}O_2$, more specifically $(Li_{0.76}Ni_{0.24})_{3b}[Ni]_{3a}O_2$, decreases rapidly below 200 K with decreasing T [10]. Indeed, it is proposed that the Ni ions in the Li layer produce an FM interaction between the adjacent NiO_2 planes, whether the additional inter-plane interaction between the Li layer and NiO_2 plane is FM or antiferromagnetic (AF) [11]. The magnetic anomalies on $LiNi_{1-x}Co_xO_2$ were also reported by other two groups. Although $LiNiO_2$ was known to exhibit a spin-glass-like transition at $T_f \sim 9$ K [12], Hirota et al. [8] reported that T_f does not vary with x systematically; that is, $T_f \sim 35$ K for $LiNiO_2$, but $T_f \sim 50$ K for the $x=0.05$ phase, and then $T_f \sim 15$ K for the $x=0.15$ phase. On the other hand, Gendron et al. [9] revealed a typical FM hysteresis

* Corresponding author. Fax: +81 561 63 6137.
E-mail address: e1089@mosk.tytlabs.co.jp (K. Mukai).

0022-4596/$ - see front matter © 2010 Elsevier Inc. All rights reserved.
doi:10.1016/j.jssc.2010.05.019

loop for the $x=0.2$ compound below 80 K. Consequently, the magnetic nature of the lightly Co-substituted $LiNiO_2$ is still controversial, despite extensive research efforts on $LiNi_{1-x}Co_xO_2$.

Recently, we investigated the macro- and microscopic magnetism for $LiNi_{1-x}Co_xO_2$ ($x=0$, 0.25, 0.5, 0.75, and 1) by both χ and muon-spin rotation/relaxation (μSR) measurements [13,14]. Here, μSR is very sensitive to local magnetic environment and is one of the powerful techniques to detect both static and dynamic internal magnetic fields caused by nuclear- and electronic-magnetic moments [15]. As x increases from 0, μ_{eff} decreased monotonously, as expected [13]. Moreover, the distribution width of internal magnetic field(s) (Δ) caused by the frozen but disordered Ni^{3+} moments was found to decrease exponentially with increasing x [13]. These results were most likely to suggest that the Co-substitution simply dilutes the magnetism of the Ni ions. In other words, both Ni and Co ions distribute homogeneously/randomly in the transition metal layer, even in a muon-scale (within a few interatomic distances). On the basis of our results, the magnetic nature of $LiNi_{1-x}Co_xO_2$ is, hence, expected to vary with x monotonically, even for the compounds with $x \leq 0.25$, in contrast to the past reports [7–9].

A comparison between the magnetic nature for the $x<0.25$ compounds [7–9] and that for the $x \geq 0.25$ compounds [13] leads to the complex/drastic change in the magnetism in the x range below 0.25, probably due to the migration of the Ni ions to the Li layer or the presence of short-range cation/magnetic order. Such migration of Ni ions or short-range order would also affect their electrochemical properties. We have, therefore, performed the structural, magnetic, and electrochemical studies for the $LiNi_{1-x}Co_xO_2$ samples with $x=0$, 0.05, 0.1, and 0.25 in detail, in order to elucidate the inter-relationship between structural, magnetic, and electrochemical properties with $x \leq 0.25$. Moreover, we discuss the possibility of $LiNi_{1-x}Co_xO_2$ for a positive electrode material for high energy-density LIB.

2. Experimental

Polycrystalline $LiNi_{1-x}Co_xO_2$ samples with $x=0$, 0.05, 0.1, and 0.25 were prepared by a solid-state reaction technique, as reported previously [3,13]. The reaction mixture of $LiNiO_3$, $NiCO_3$, and $CoCO_3$ was well mixed and pressed into a pellet of 23 mm diameter and $\sim$5 mm thickness. The pellet was heated at 650 °C in an oxygen flow for 12 h, and then ground and pressed into a pellet again. Finally, the pellet was fired at 750 °C in oxygen flow for 12 h. The obtained $LiNi_{1-x}Co_xO_2$ powders were characterized by a powder X-ray diffraction (XRD, RINT-2200, Rigaku Co. Ltd., Japan) measurement and electrochemical charge and discharge test in a non-aqueous lithium cell. The Li/Ni/Co ratios were determined to be 0.97/1.00/0 for $x=0$, 1.01/0.95/0.05 for $x=0.05$, 1.02/0.90/0.10 for $x=0.1$, and 1.04/0.76/0.24 for $x=0.25$, by an inductively coupled plasma-atomic emission spectral (ICP-AES, CIROS 120, Rigaku Co. Ltd., Japan) analysis.

The electrochemical reactivity was examined in a non-aqueous lithium cell. In preparing the electrodes, polyvinylidene fluoride (PVdF) dissolved in *N*-methyl-2-pyrrolidone (NMP) solution was used as a binder. The black viscous slurry consisting of 88 wt% $LiNi_{1-x}Co_xO_2$ powder, 6 wt% acetylene black, and 6 wt% PVdF was cast on an aluminum foil with blade. NMP was evaporated at 120 °C for 30 min, and finally the electrodes ($\varnothing$15 mm) were dried under vacuum at 150 °C for 12 h. The lithium metal sheet pressed on a stainless steel plate ($\varnothing$19 mm) was used as a counter electrode. Two sheets of porous polypropylene membrane (Celgard 2500) were used as a separator. The electrolyte was 1 M $LiPF_6$ dissolved in ethylene carbonate (EC)/diethyl carbonate (DMC) (3/7 volume ratio) solution.

χ was measured using a superconducting quantum interference device (SQUID) magnetometer (MPMS, Quantum Design) in the T range between 5 and 400 K under magnetic field $H \leq 55$ kOe. χ was also measured in the T range between 2 and 100 K with $H=10$ and 100 Oe in both zero-field-cooling (ZFC) and field-cooling (FC) modes. First, the sample was cooled in ZF from 100 K, then a magnetic field was applied, and finally χ_{ZFC} was measured with increasing T from 5 (2) to 100 K. Subsequently, χ_{FC} was measured with decreasing T from 100 to 5 (2) K. Electron spin resonance (ESR) spectra were recorded by a ESP300E (Bruker) spectrometer in the T range between 100 and 300 K. The gyromagnetic (g) factor of Ni and Co ions was determined with respect to a MnO/MgO standard.

3. Results

3.1. Crystal structure of $LiNi_{1-x}Co_xO_2$

The crystal structure of the $LiNi_{1-x}Co_xO_2$ samples with $x=0$, 0.05, 0.1, and 0.25 was well assigned as a layered structure with space group $R\bar{3}m$. A small amount of Ni ions is, however, known

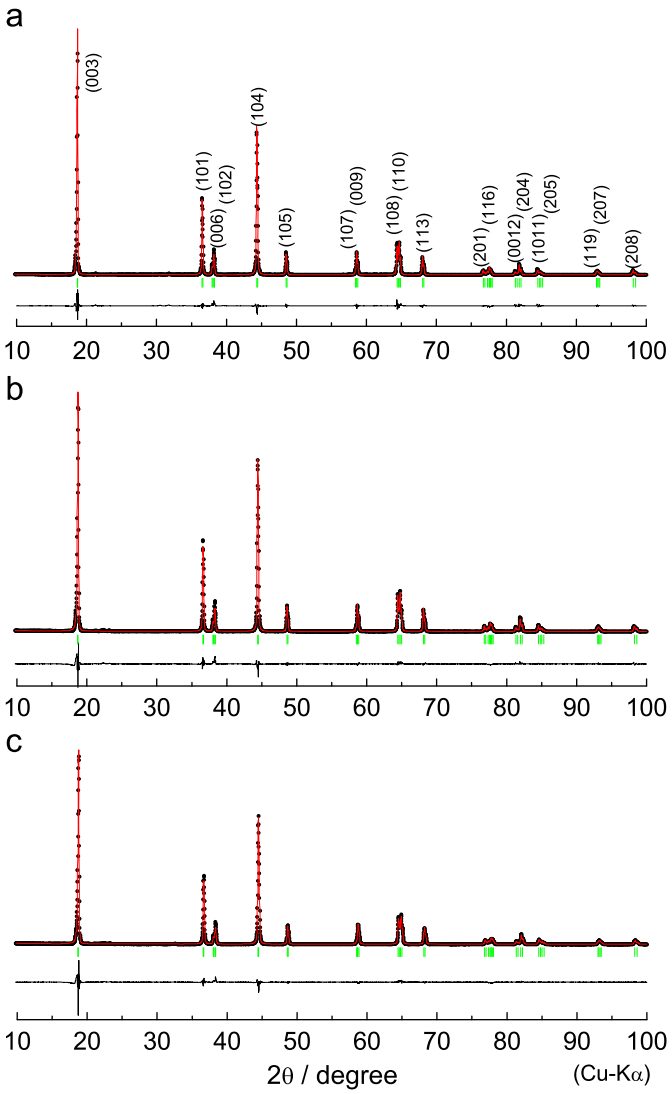

Fig. 1. Rietveld analysis for the $LiNi_{1-x}Co_xO_2$ samples with (a) $x=0$, (b) 0.05, and (c) 0.1. The observed (I_{obs}) and calculated (I_{calc}) intensity data are plotted as points and solid line in the upper field. The bar-code type indications show all the possible Bragg reflections. The difference between I_{obs} and I_{calc} is shown in the lower field.

to unavoidably migrate from 3*a* site to 3*b* (Li) site especially for $x \leq 0.2$ [16]. A Rietveld analysis with RIETAN2000 [17] was, therefore, performed in order to estimate the amount of the Ni ions at the 3*b* site, i.e. δ in $(Li_{1-\delta}Ni_{\delta})_{3b}[Ni_{1-x-\delta}Co_x]_{3a}O_2$. Fig. 1 shows the results of the Rietveld analysis for the $LiNi_{1-x}Co_xO_2$ samples with (a) $x=0$, (b) $x=0.05$, and (c) $x=0.1$. First, we assumed a perfectly ordered structure with $\delta=0$. This structural model yielded a negative isotropic atomic displacement parameter for the Li ion [B_{iso}(Li)]. This means that the real electron density at the 3*b* site is higher than the expected [16]. The Rietveld analysis was, hence, performed under the assumption that the Ni ions occupy both 3*a* and 3*b* sites, while the Li ions locate only at the 3*b* site and the Co ions at the 3*a* sites. Moreover, we assume that there is no oxygen deficiency in the samples as reported previously [3,16,18]. This is because the formal charge of oxygen ion in $LiNiO_2$ is already reported to be -2 by an electron energy loss spectroscopy (EELS) analysis [19]. The lattice parameters of a_h- and c_h-axes decrease almost linearly with increasing *x*, as will be seen in Fig. 6. On the other hand, the amount of δ for the three samples was found to be ~ 0.01, indicating that δ is independent of *x* (see Table 1). Here, we should naturally note the accuracy of δ estimated by XRD data. For the change of δ with *x* will be discussed later using the magnetization data.

3.2. Magnetic property of $LiNi_{1-x}Co_xO_2$

Fig. 2 shows the *T* dependences of χ ($=M/H$) and χ^{-1} for the $LiNi_{1-x}Co_xO_2$ samples with $x=0$, 0.05, 0.1, and 0.25 measured in FC mode with $H=10$ kOe. Although the appearance of either an FM or ferrimagnetic component was reported below ~ 200 K for the $x=0.05$, 0.1, and 0.25 compounds [7], χ^{-1} decreases monotonically with decreasing *T* down to ~ 100 K, indicating a Curie–Weiss (CW) PM behavior. For the PM state, a CW law in the general form is written as

$$\chi = \frac{N\mu_{eff}^2}{3k_B(T-\Theta_p)} + \chi_0, \quad (1)$$

where k_B is the Boltzmann's constant, *T* is the absolute temperature, Θ_p is the Weiss temperature, *N* is the number density of Ni and Co ions, μ_{eff} is the effective magnetic moment of Ni and Co ions, and χ_0 is the *T*-independent susceptibility. Using Eq. (1) in the *T* range between 200 and 400 K, we obtain the values of μ_{eff} and Θ_p for the $LiNi_{1-x}Co_xO_2$ samples (see Table 2). The value of μ_{eff}^{pre}, which is the predicted μ_{eff} for the case that Ni^{3+} ions in a low-spin state with $S=1/2$ ($t_{2g}^6e_g^1$), Co^{3+} ions with $S=0$ (t_{2g}^6), and the *g*-factor of both ions is 2, is also listed in Table 2. The observed μ_{eff} is larger than μ_{eff}^{pre}, but note that the present deviation of μ_{eff} from μ_{eff}^{pre} is significantly small compared with that reported in Ref. [7]. The discrepancy between μ_{eff} and μ_{eff}^{pre} is partially attributed to an enhancement of the *g*-factor caused by a local Jahn–Teller (JT) distortion of the NiO_6-octahedron, as in the case for $NaNiO_2$ [20] and Ag_2NiO_2 [21]. In fact, ESR measurements showed that the *g*-factor for $LiNiO_2$ is 2.13 ± 0.03 in the *T* range between 100 and 300 K, which is almost consistent with the past result for $LiNiO_2$ ($g=2.17$) [22]. The other contribution for the deviation from μ_{eff}^{pre} would come from spin-orbit couplings through the Landé *g*-factor in the expression of $\mu_{eff}=g\sqrt{J(J+1)}$. Here, *J* is the total angular momentum consists of the spin *S* and the orbital *L* angular momenta.

As seen in Fig. 2(a), as *T* decreases from 400 K, χ for all the samples rapidly increases below ~ 100 K, indicating the presence of localized Ni moments. In order to elucidate the magnetic behavior below ~ 100 K, Fig. 3 shows the *T* dependence of χ for the $LiNi_{1-x}Co_xO_2$ samples with (a) $x=0$, (b) $x=0.05$, (c) $x=0.1$, and (d) $x=0.25$, measured in both ZFC and FC modes with $H=10$ and 100 Oe. For the $x=0.05$ sample, the $\chi_{FC}(T)$ curve almost traces the $\chi_{ZFC}(T)$ curve down to ~ 10 K, and then deviates from the $\chi_{ZFC}(T)$ curve with further lowering *T*. Both $\chi_{FC}(T)$ and $\chi_{ZFC}(T)$ curves show a maximum around 9.6 K, indicating the occurrence of a spin-glass-like transition at $T_f=9.6$ K. The $\chi(T)$ curves for the $x=0.1$ and 0.25 samples are essentially the same with those for the $x=0.05$ sample, except for the magnitude of χ and T_f ($T_f=8.4$ K for the $x=0.1$ sample and $T_f=4.8$ K for the $x=0.25$ sample). On the contrary, the $\chi_{FC}(T)$ curve for $LiNiO_2$ deviates from the $\chi_{ZFC}(T)$ curve

Table 1
The structural parameters determined by the Rietveld analysis for the $LiNi_{1-x}Co_xO_2$ samples with $x=0$, 0.05, and 0.1.

Sample	Space group	Atom	Wyckoff position	Occupancy (g_{occ})[a]	*X*	*Y*	*Z*	B_{iso}[b]/Å^2
$x=0$	$R\bar{3}m$	Li	3*b*	0.990(2)	0	0	1/2	0.5(2)
		Ni1	3*b*	0.010(2)	0	0	1/2	0.5(2)
		Ni2	3*a*	0.990(2)	0	0	0	0.58(2)
		O	6*c*	1.0	0	0	0.259(2)	1.39(4)
$a_h=2.8786(1)$ Å and $c_h=14.1984(2)$ Å								
$R_{wp}=9.68$, $R_B=2.80$, and $S=2.71$								
$x=0.05$	$R\bar{3}m$	Li	3*b*	0.989(2)	0	0	1/2	0.5(2)
		Ni1	3*b*	0.007(2)	0	0	1/2	0.5(2)
		Ni2	3*a*	0.943(2)	0	0	0	0.48(2)
		Co	3*a*	0.05	0	0	0	0.48(2)
		O	6*c*	1.0	0	0	0.259(1)	1.23(5)
$a_h=2.8747(1)$ Å and $c_h=14.1852(2)$ Å								
$R_{wp}=10.85$, $R_B=2.79$, and $S=2.49$								
$x=0.1$	$R\bar{3}m$	Li	3*b*	0.989(2)	0	0	1/2	0.5(2)
		Ni1	3*b*	0.009(2)	0	0	1/2	0.5(2)
		Ni2	3*a*	0.891(2)	0	0	0	0.46(2)
		Co	3*a*	0.1	0	0	0	0.46(2)
		O	6*c*	1.0	0	0	0.259(1)	1.23(5)
$a_h=2.8717(1)$ Å and $c_h=14.1811(3)$ Å								
$R_{wp}=10.97$, $R_B=3.26$, and $S=2.31$								

[a] Constrains : g_{occ}(Ni1) + g_{occ}(Ni2)=1 for $x=0$, g_{occ}(Ni1) + g_{occ}(Ni2)=0.95 for $x=0.05$, g_{occ}(Ni1) + g_{occ}(Ni2)=0.9 for $x=0.1$, and g_{occ}(Li)=1−g_{occ}(Ni1).
[b] Constrains : B (Li)=B(Ni1) and B(Ni2)=B(Co).

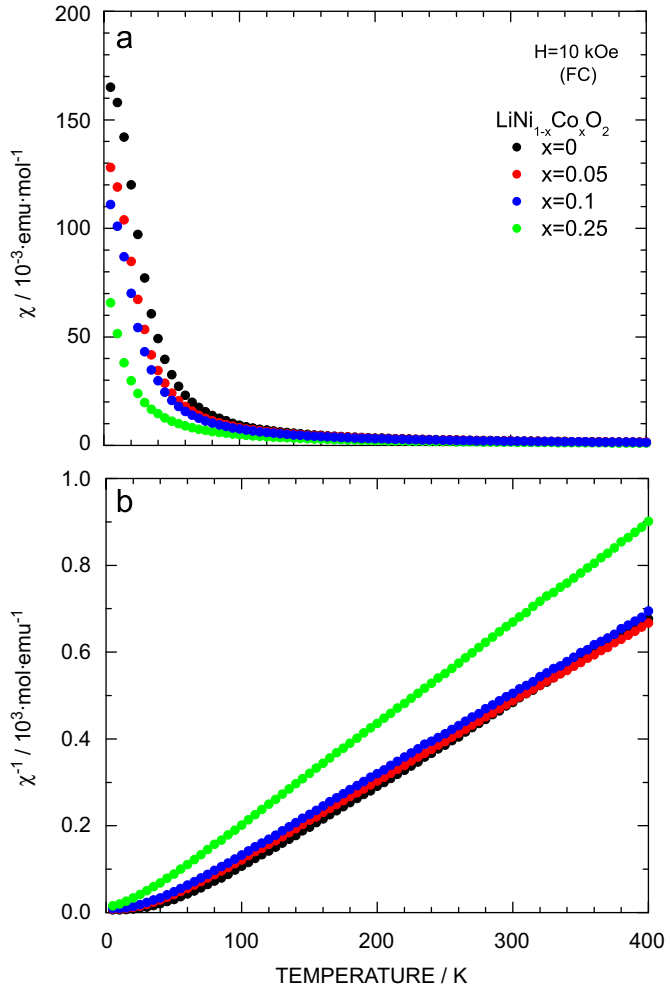

Fig. 2. (a) Magnetic susceptibility (χ) and (b) inverse susceptibility (χ^{-1}) for the $LiNi_{1-x}Co_xO_2$ samples with $x=0$, 0.05, 0.1, and 0.25 measured with field-cooling (FC) mode with $H=10$ kOe.

Table 2
The effective magnetic moment (μ_{eff}), Weiss temperature (Θ_p), T-independent susceptibility (χ_0), predicted effective magnetic moment (μ_{eff}^{pre}), and gyromagnetic (g) factor for the $LiNi_{1-x}Co_xO_2$ samples with $x=0$, 0.05, 0.1, and 0.25.

x	μ_{eff} (μ_B)	Θ_p (K)	$\chi_0 \times 10^{-3}$ (emu mol^{-1})	μ_{eff}^{pre} (μ_B)[a]	g-factor[b]
0	2.02(3)	51(2)	0.02(2)	1.73	2.13(3)
0.05	2.03(3)	41(2)	0.07(1)	1.69	2.07(3)
0.1	2.06(3)	28(2)	0.02(2)	1.63	2.05(3)
0.25	1.84(4)	14(3)	0.01(2)	1.50	2.06(5)

[a] μ_{eff}^{pre} was calculated by assuming that Ni^{3+} ions and Co^{3+} ions are in the low-spin state with $S=\frac{1}{2}$ ($t_{2g}^6e_g^1$) and $S=0$ (t_{2g}^6), respectively, and $g=2$.
[b] The g-factor was determined by ESR measurements.

far above its T_f (=10.8 K). The low-H measurements at 10 Oe enhances the deviation between the $\chi_{FC}(T)$ and $\chi_{ZFC}(T)$ curves, as expected. Furthermore, there is a small cusp in the $\chi(T)$ curves around 30 K. According to the past magnetic studies on $LiNiO_2$ with $H=10$ Oe, T_f is ~50 K for the $(Li_{0.95}Ni_{0.05})_{3b}[Ni_{0.95}]_{3a}O_2$ compound ($\delta=0.05$)[23] and T_f is ~40 K for the $(Li_{0.96}Ni_{0.04})_{3b}$ $[Ni_{0.96}]_{3a}O_2$ compound ($\delta=0.04$) [24]. Therefore, the difference between the $\chi_{FC}(T)$ and $\chi_{ZFC}(T)$ curves above T_f and the cusp near 30 K are not due to a formation of magnetic order but due to a small amount of the FM components (below a few %) caused by the Ni ions at the 3b site. Indeed, our μSR measurements on $LiNiO_2$ demonstrated that $LiNiO_2$ is entirely in a PM state down to ~18 K [14].

In the ideal $LiNiO_2$ lattice, only the approximately 90° Ni–O–Ni bonds exist in the NiO_2 planes. However, the actual ionic distribution of $LiNiO_2$ is represented as $(Li_{1-\delta-\omega}Ni_{\delta+\omega}^{2+})_{3b}$ $[Ni_{1-\delta}^{3+}Ni_{\delta-\omega}^{2+}Li_\omega]_{3a}O_2$ [18], due to the presence of the Ni ions in the Li layer. The Ni ions in the Li layer are, thus, considered to introduce the FM component in the $LiNi_{1-x}Co_xO_2$ samples, based on Goodenough–Kanamori rules [25]. Fig. 4 shows the M versus H curves at (a) 20 K and (b) 5 K for the $LiNi_{1-x}Co_xO_2$ samples with $x=0$, 0.1, 0.05, and 0.25, in order to check the amount of the FM component. Although a M–H loop is clearly observed for the samples with $x \leq 0.1$, the shape of the loop is not a typical FM-like, but a ferrimagnetic-like, both above and below T_f. That is, as H increases from 0 kOe, M rapidly increases with changing its slope (dM/dH) up to ~20 kOe, then increases almost linearly with further increasing H. Moreover, the remanent magnetization M_r, i.e. M at $H=0$ kOe is less than 2 emu mol^{-1} for all the samples at 20 K, and 16, 8, and 5 emu mol^{-1} for the $x=0$, 0.05, and 0.1 samples, respectively, at 5 K (see inset in Fig. 4). Note that M_r at 5 K is dominated by a contribution of spin-glass-like order, because the M–H loop shown in Fig. 4(b) is usually observed for a spin-glass-like phase. Since M_r (20 K) is almost independent of x, the amount of δ is considered to be not significantly altered with x. This consideration is consistent with the result of Rietveld analyses (see Fig. 1 andTable 1).

3.3. Electrochemical properties of $LiNi_{1-x}Co_xO_2$

Fig. 5 shows the charge and discharge (C/D) curves of the $Li/LiNi_{1-x}Co_xO_2$ cells with (a) $x=0$, (b) 0.05, (c) 0.1, and (d) 0.25. The cells were operated at a current density of 0.17 mA cm^{-2} at 25 °C in the voltage range between 2.6 and 4.2 V. The C/D curves for $LiNiO_2$ exhibit a couple voltage plateau around 3.6, 4.0, and 4.2 V, indicating that the crystal structure of Li_yNiO_2 varies with y [3]. That is, as y decreases from 1, a rhombohedral ($R\bar{3}m$) phase is stable down to ~0.75, whereas a monoclinic (C 2/m) phase is stable in the y range between 0.75 and ~0.45. Then, a rhombohedral ($R\bar{3}m$) phase appears again for 0.45 $\geq y >$ 0.25, and finally two rhombohedral ($R\bar{3}m$) phases coexist for 0.25 $\geq y >$ ~0.1. The voltage plateaus are also seen in the C/D curves for the $x=0.05$ and 0.1 samples, while the C/D curves for the $x=0.25$ sample show a continuous change in voltage. Surprisingly, the steady discharge capacity (Q_{dis}) for the $x=0.05$ and 0.1 samples are larger than that for the $x=0$ sample; namely, $Q_{dis}=180$ mAh g^{-1} for $x=0$, $Q_{dis}=217$ mAh g^{-1} for $x=0.05$, and $Q_{dis}=206$ mAh g^{-1} for $x=0.1$. This is because the irreversible capacity (Q_{irre}) at the initial cycle drastically decreases with the substitution of Co ions $Q_{irre}=40$ mAh g^{-1} for $x=0$, $Q_{irre}=20$ mAh g^{-1} for $x=0.05$, and $Q_{irre}=15$ mAh g^{-1} for $x=0.1$.

4. Discussion

4.1. Comparison with the past magnetic studies on $LiNi_{1-x}Co_xO_2$

According to past work, either an FM or a ferrimagnetic component appeared below ~200 K for the $LiNi_{1-x}Co_xO_2$ compounds with $x=0.05$, 0.1 and 0.15 [7]. And, $\mu_{eff}=2.61\,\mu_B$ for the $x=0.05$ compound, and $2.59\,\mu_B$ for the $x=0.1$ compound, if we calculate μ_{eff} using the Curie constant in Ref. [7] and $g=2$. On the other hand, Hirota et al. [8] reported a complex x dependence of T_f; namely, the presence of the maximum of T_f (=50 K) at $x=0.05$. Gendron et al. [9] showed a typical FM hysteresis loop for the $x=0.2$ compound with a saturation magnetization M_s ~1100 emu mol^{-1} at 40 K. Such phenomena have never been observed for the present samples, but their structural and magnetic properties are found to vary monotonically with x (see

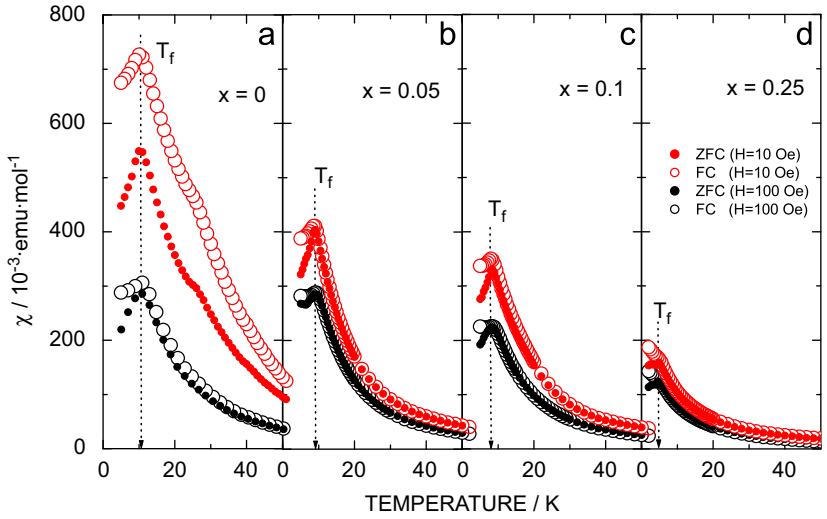

Fig. 3. Temperature dependence of magnetic susceptibility (χ) for the $LiNi_{1-x}Co_xO_2$ samples with (a) $x=0$, (b) $x=0.05$, (c) $x=0.1$, and (d) $x=0.25$. χ was measured in both zero-field-cooling (ZFC) and field-cooling (FC) modes with $H=10$ and 100 Oe. T_f represents the spin-glass-like transition temperature.

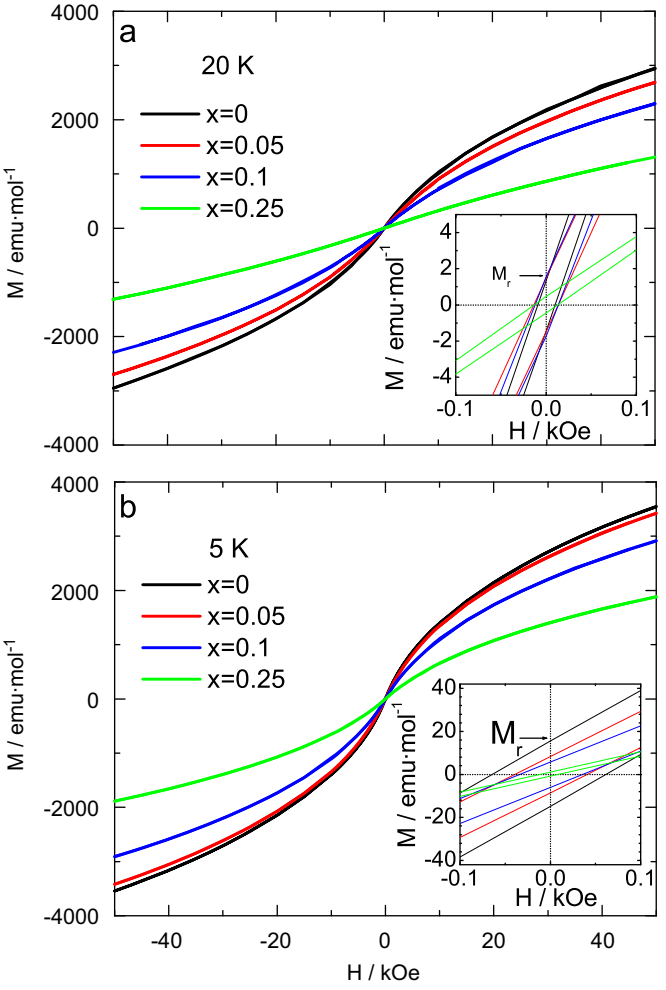

Fig. 4. Magnetization (M) as a function of field (H) at (a) 20 K and (b) 5 K for the $LiNi_{1-x}Co_xO_2$ samples with $x=0$, 0.1, 0.05, and 0.25. The enlarged M–H curve was also shown in the inset. M_r represents the remanent magnetization, i.e. M at $H=0$ kOe.

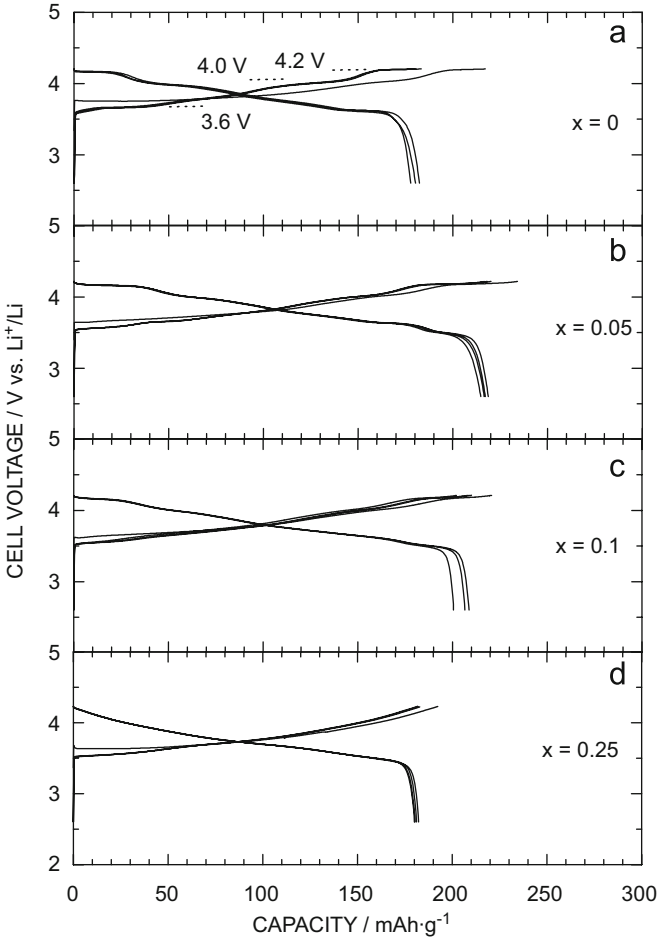

Fig. 5. Charge and discharge curves of the $Li/LiNi_{1-x}Co_xO_2$ cells with (a) $x=0$, (b) 0.05, (c) 0.1, and (d) 0.25. The cells were operated at a current density of 0.17 mA cm^{-2} at 25 °C in the voltage range between 2.6 and 4.2 V.

Figs. 1–4 and Tables 1 and 2). This situation is more clearly seen in Fig. 6, in which the x dependences of the lattice parameters, μ_{eff}, Θ_p, and T_f are shown. It should be also emphasized that the present variation of the physical properties with x is very consistent with our previous result on the $x=0$, 0.25, 0.5, 0.75, and 1 samples [13]. On the contrary, since the Ni moments are

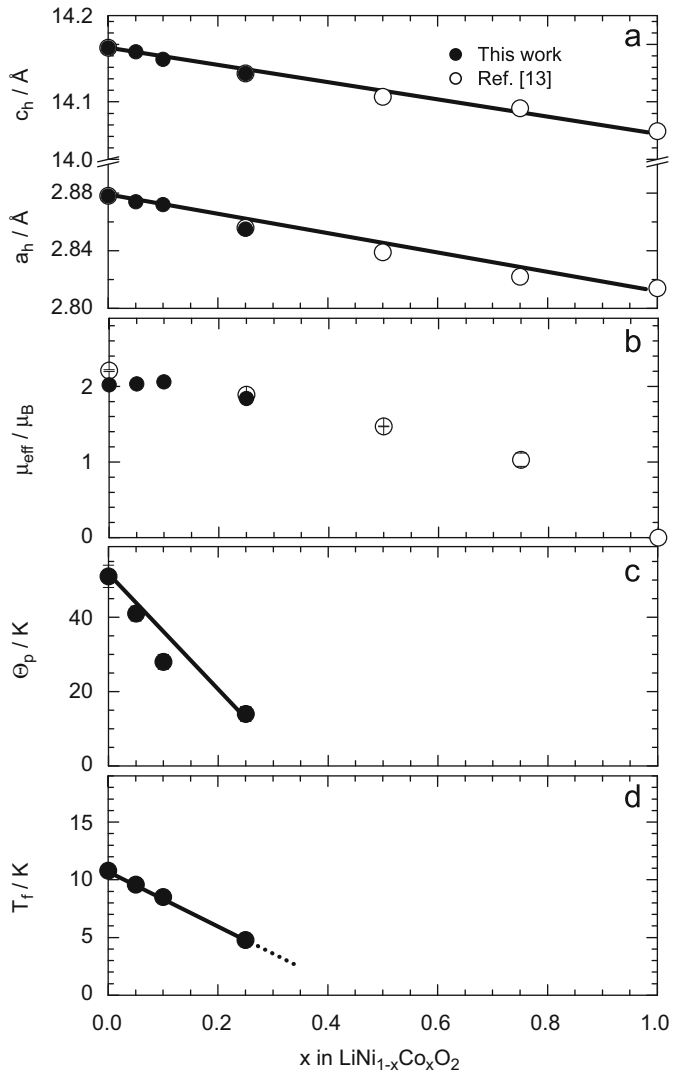

Fig. 6. x dependences of the (a) lattice parameters of a_h- and c_h-axes, (b) effective magnetic moment (μ_{eff}), (c) Weiss temperature (Θ_p), and (d) spin-glass-like transition temperature (T_f) for the $LiNi_{1-x}Co_xO_2$ samples. The previously reported values of lattice parameters and μ_{eff} in Ref. [13] are also shown for comparison.

simply diluted by Co ions with x, it is very difficult to explain the existence of a local maximum of T_f at around $x=0.05$. Thus, the magnetic nature for the present $LiNi_{1-x}Co_xO_2$ samples with $x<0.25$ is found to be very different from those for the previously reported $LiNi_{1-x}Co_xO_2$ [7–9].

Here, we should note that the present $LiNi_{1-x}Co_xO_2$ samples were prepared at 750 °C, while the past work used the samples synthesized at 800 [7,9] and 850 °C [8]. The heat treatment above 800 °C were, however, known to be not an optimal condition to obtain the ideal layered structure with $R\bar{3}m$ [3,10]. Furthermore, the $\chi^{-1}(T)$ curve for $LiNi_{0.95}Mg_{0.05}O_2$, in which the Ni ions locate only at the 3a site, exhibits a typical CW behavior down to ~50 K with $T_f \sim 8$ K [26]. Therefore, the magnetic properties of $LiNi_{1-x}Co_xO_2$ is thought to be strongly affected by their synthesis condition, i.e. δ. Indeed, M_r for $(Li_{0.94}Ni_{0.06})_{3b}[Ni]_{3a}O_2$ at 5 K are reported to be ~500 emu mol^{-1} due to the large amount of δ [27].

4.2. Inter-relationship between structural, magnetic, and electrochemical properties of $LiNi_{1-x}Co_xO_2$

Saadoune and Delmas showed the electrochemical properties of $LiNi_{1-x}Co_xO_2$ in the voltage range between 2.5 and 4.0 V [7]. The Q_{dis} for the $x=0$, 0.1, and 0.2 compounds is ~137, 104, and 151 mAh g^{-1}, respectively, while the Q_{irre} for the $x=0$, 0.1, and 0.2 compounds is ~27, 33, and 16 mAh g^{-1}, respectively [7]. As seen in Fig. 5, the Q_{dis} for the $x=0.05$ and 0.1 samples are larger than that for the $x=0$ sample. Furthermore, a light substitution for Ni by Co ($x=0.05$) is found to be suppressed Q_{irre} by ~20 mAh g^{-1}. Here, the applied current density in Ref. [7] (=0.07 mA cm^{-1}; C/200) is much lower than that in the present study (=0.17 mA cm^{-1}; ~C/10). Combining the results on magnetic measurements, the difference between the previous [7] and present studies in the electrochemical properties is most likely due to the difference in the amount of δ. Actually, the value of δ for the $x=0.1$ compound which is synthesized at 800 °C is reported to be 0.027(5) by Delmas and co-workers [16] and is significantly larger than that for the present $x=0.1$ sample (=0.009).

The origin of the increase in Q_{dis} with x is currently unclear, because the structural and magnetic analyses indicated that the amount of δ is almost independent on x (Table 1 and Fig. 4). In addition, the charge end voltage of 4.2 V versus Li$^+$/Li would affect the Q_{dis}, because the operating voltage is extremely flat around 4.2 V (Fig. 5) due to the structural change between the two rhombohedral ($R\bar{3}m$) phases [3]. It is, however, noteworthy the result of $LiNi_{1-x}Mg_xO_2$ [28]. The amount of δ in $(Li_{1-x-\delta}Ni_\delta Mg_x)_{3b}[Ni_{1-x-\delta}]_{3a}O_2$ is known to decrease by the substitution for Ni by Mg and reach 0 at $x=0.02$ by XRD and magnetic measurements [28]. Nevertheless, the Q_{dis} in the voltage range between 2.6 and 4.15 V for $LiNi_{1-x}Mg_xO_2$ monotonically decreases with x [28]; namely, $Q_{dis} \sim 167$ mAh g^{-1} for $LiNiO_2$, $Q_{dis} \sim 165$ mAh g^{-1} for the $LiMg_{0.01}Ni_{0.99}O_2$ compound, $Q_{dis} \sim 156$ mAh g^{-1} for the $LiMg_{0.02}Ni_{0.98}O_2$ compound, and $Q_{dis} \sim 135$ mAh g^{-1} for the $LiMg_{0.05}Ni_{0.95}O_2$ compound. On the other hand, the Q_{dis} for $LiNi_{1-x}Co_xO_2$ in the voltage range between 2.6 and 4.15 V is estimated as 155 mAh g^{-1} for $x=0$, 182 mAh g^{-1} for $x=0.05$, and 188 mAh g^{-1} for $x=0.1$. This indicates that the light substitution by transition metal ions play a significant role for determining the Q_{dis}.

Finally, we wish to discuss the possibility for a positive electrode material for high energy-density LIB. Table 3 summarizes the Q_{dis}, energy density (W), and average voltage (E_{ave}) for the $LiNi_{1-x}Co_xO_2$ samples with $x=0$, 0.05, and 0.1 obtained from the discharge curve at the second cycle. The values of W for the $x=0.1$ and 0.05 samples are almost comparable to that for $LiNi_{1/2}Mn_{1/2}O_2$ ($W \sim 770$ Ah g^{-1}) [29] or $LiCo_{1/3}Ni_{1/3}Mn_{1/3}O_2$ ($W \sim 800$ Ah g^{-1}) [30]. Note that W for $LiNi_{1/2}Mn_{1/2}O_2$ is estimated from the discharge curve in the voltage range between 2.5 and 4.5 V [29], while that for $LiCo_{1/3}Ni_{1/3}Mn_{1/3}O_2$ from the discharge curve in the voltage range between 2.5 and 4.6 V [30]. It is widely known that, in the voltage level above 4.2 V, a non-aqueous electrolyte gradually decomposes electrochemically, resulting in capacity fading during charge and discharge cycles, especially at temperatures above 60 °C. Therefore, the lightly substituted $LiNi_{1-x}Co_xO_2$ is promising as a positive electrode material for LIB with high energy-density, when we set the charge end voltage as 4.2 V.

Table 3
The discharge capacity (Q_{dis}), energy density (W), and average voltage (E_{ave}) for $LiNi_{1-x}Co_xO_2$.[a]

x	Q_{dis} (mAh g^{-1})	W (Ah g^{-1})	E_{ave} (V)
0	180	667	3.81
0.05	217	829	3.82
0.1	206	785	3.81

[a] The values of Q_{dis}, W, and E_{ave} were obtained from the discharge curve in the voltage range between 2.6 and 4.2 V.

5. Conclusion

The inter-relationship between the structural, magnetic. and electrochemical properties for the $LiNi_{1-x}Co_xO_2$ samples with $x=0$, 0.05, 0.1 and 0.25 was investigated by powder X-ray diffraction measurements, magnetic susceptibility (χ) measurements, and electrochemical charge and discharge test. For all the samples, the temperature (T) dependence of χ^{-1} measured with the magnetic field with $H=10$ kOe exhibited a typical Curie–Weiss behavior down to 100 K. Below 100 K, an antiferromagnetic correlation is likely to be enhanced, since the slope of the $\chi^{-1}(T)$ curve is more moderate than that above 100 K. At low T, all the samples entered into a spin-glass-like phase below T_f. The magnitude of T_f, effective magnetic moment, and Weiss temperature were found to vary almost linearly with x. Furthermore, the electrochemical measurements showed that the discharge capacities for $x=0.05$ and 0.1 are larger than that for $x=0$. Therefore, the magnetic and electrochemical properties for the present $LiNi_{1-x}Co_xO_2$ samples is found to be very different from those for previously reported [7–9], probably due to the difference in the amount of Ni ions in the Li layer. In order to obtain the highly crystallized $LiNi_{1-x}Co_xO_2$ compounds with $x \leq 0.25$, we need employ high-T synthesis as in the case for $LiCoO_2$. However, high-T synthesis induce the migration of Ni ions in the Li layer. Since the amount of Ni ions in the Li layer strongly depends on the magnetic parameters such as T_f and Weiss temperature, magnetic studies are considered to be effective for determining the optimum synthesis conditions of lightly substituted $LiNi_{1-x}Co_xO_2$.

Acknowledgments

We appreciate S. Kohno and K. Ariyoshi of Osaka City University for preparation and electrochemical characterization of $LiNi_{1-x}Co_xO_2$. We also thank Y. Kondo of TCRDL for ICP-AES analysis. This work is partially supported by Grant-in-Aid for Scientific Research (B), 1934107, MEXT, Japan.

References

[1] G. Pistoia, Lithium Batteries, Elsevier, Amsterdam, 1993.
[2] J.R. Dahn, U. von Sacken, M.W. Juzkow, H. Al-Janaby, J. Electrochem. Soc. 138 (1991) 2207–2211.
[3] T. Ohzuku, A. Ueda, M. Nagayama, J. Electrochem. Soc. 140 (1993) 1862–1870.
[4] C. Delmas, I. Saadoune, Solid State Ionics 53–56 (1992) 370–375.
[5] T. Ohzuku, K. Nakura, T. Aoki, Electrochim. Acta 45 (1999) 151–160.
[6] T. Ohzuku, A. Ueda, M. Nagayama, Y. Iwakoshi, H. Komori, Electrochim. Acta 38 (1993) 1159–1167.
[7] I. Saadoune, C. Delmas, J. Mater. Chem. 6 (1996) 193–199.
[8] K. Hirota, H. Yoshizawa, M. Ishikawa, J. Phys. Condens. Matter. 4 (1992) 6291–6302.
[9] F. Gendron, S. Castro-Garcia, E. Popova, S. Ziolkiewicz, F. Soulette, C. Julien, Solid State Ionics 157 (2003) 125–132.
[10] A. Rougier, P. Gravereau, C. Delmas, J. Electrochem. Soc. 143 (1996) 1168–1175.
[11] M.J. Lewis, B.D. Gaulin, L. Filion, C. Kallin, A.J. Berlinsky, H.A. Dabkowska, Y. Qiu, J.R.D. Copley, Phys. Rev. B 72 (2005) 014408.
[12] J.N. Reimers, J.R. Dahn, J.E. Greedan, C.V. Stager, G. Liu, I. Davidson, U. Von Sacken, J. Solid State Chem. 102 (1993) 542–552.
[13] K. Mukai, J. Sugiyama, Y. Ikedo, J.H. Brewer, E.J. Ansaldo, G.D. Morris, K. Ariyoshi, T. Ohzuku, J. Power Sources 174 (2007) 843–846.
[14] J. Sugiyama, K. Mukai, Y. Ikedo, P.L. Russo, H. Nozaki, D. Andreica, A. Amato, K. Ariyoshi, T. Ohzuku, Phys. Rev. B 78 (2008) 144412.
[15] A. Schenck, Muon Spin Rotation Spectroscopy Principles and Applications in Solid State Physics, Adam Hilger, Bristol, 1985.
[16] A. Rougier, I. Saadoune, P. Gravereau, P. Willmann, C. Delmas, Solid State Ionics 90 (1996) 83–90.
[17] F. Izumi, T. Ikeda, Mater. Sci. Forum 198 (2000) 321–324.
[18] C. Pouillerie, E. Suard, C. Delmas, J. Solid State Chem. 158 (2001) 187–197.
[19] Y. Koyama, T. Mizoguchi, H. Ikeno, I. Tanaka, J. Phys. Chem. B 109 (2005) 10749–10755.
[20] E. Chappel, M.D. Núñez-Regueiro, G. Chouteau, O. Isnard, C. Darie, Eur. Phys. J. B 17 (2000) 615–622.
[21] H. Yoshida, Y. Muraoka, T. Sörgel, M. Jansen, Z. Hiroi, Phys. Rev. B 73 (2006) 020408(R).
[22] E. Chappel, M.D. Núñez-Regueiro, S. de Brion, G. Chouteau, V. Bianchi, D. Caurant, N. Baffier, Phys. Rev. B 66 (2002) 132412.
[23] A. Hirano, R. Kanno, Y. Kawamoto, Y. Takeda, K. Yamaura, M. Takano, K. Ohyama, M. Ohashi, Y. Yamaguchi, Solid State Ionics 78 (1995) 123–131.
[24] K. Yamaura, M. Takano, A. Hirano, R. Kanno, J. Solid State Chem. 127 (1996) 109–118.
[25] J.B. Goodenough, Magnetism and the Chemical Bond, Wiley, New York, 1963.
[26] M. Bonda, M. Hozapfel, S. de Brion, C. Darie, T. Fehér, P.J. Baker, T. Lancaster, S.J. Blundell, F.L. Pratt, Phys. Rev. B 78 (2008) 104409.
[27] M. Guilmard, A. Rugier, M. Grüne, L. Croguennec, C. Delmas, J. Power Sources 115 (2003) 305–314.
[28] C. Pouillerie, L. Croguennec, Ph. Biensan, C. Delmas, J. Electrochem. Soc. 147 (2000) 2061–2069.
[29] T. Ohzuku, Y. Makimura, Chem. Lett. 7 (2001) 744–745.
[30] T. Ohzuku, Y. Makimura, Chem. Lett. 7 (2001) 642–643.